

# Thermally stable sol-gel yttrium aluminum garnet cerium phosphors for white light-emitting diodes

Phan Xuan Le<sup>1</sup>, Nguyen Thi Phuong Loan<sup>2</sup>, Nguyen Doan Quoc Anh<sup>3</sup>, Hsiao-Yi Lee<sup>4</sup>

<sup>1</sup>Faculty of Electrical Engineering Technology, Industrial University of Ho Chi Minh City, Ho Chi Minh City, Vietnam

<sup>2</sup>Faculty of Fundamental 2, Posts and Telecommunications Institute of Technology, Ho Chi Minh City, Vietnam

<sup>3</sup>Faculty of Electrical and Electronics Engineering, Ton Duc Thang University, Ho Chi Minh City, Vietnam

<sup>4</sup>Department of Electrical Engineering, National Kaohsiung University of Science and Technology, Kaohsiung City, Taiwan

## Article Info

### Article history:

Received Apr 22, 2025

Revised Sep 29, 2025

Accepted Nov 07, 2025

### Keywords:

Atomic layer deposition

Sol-gel composites

Spray thermolysis

Thermal stability

Titanium dioxide

White light-emitting diodes

## ABSTRACT

This study aims to develop structurally controlled TiO<sub>2</sub>-based materials that serve a dual purpose as high-performance photocatalysts and optical scattering agents for white light-emitting diodes (LEDs). Hollow spherical TiO<sub>2</sub>, TiO<sub>2</sub>/Ag, and TiO<sub>2</sub>/Au particles were synthesized via a one-step spray thermolysis process using aqueous titanium citrate and titanium oxalate precursors. The method enables precise control of morphology and crystalline phase composition, producing hollow microspheres with tunable anatase-rutile ratios (10–100%) and crystallite sizes ranging from 12 to 120 nm. Photocatalytic performance, evaluated through the ultraviolet (UV)-driven oxidation of methylene blue, showed that as-prepared TiO<sub>2</sub> exhibited comparable activity to Degussa P25, while metal doping accelerated the anatase-to-rutile transition with minimal plasmonic enhancement under UV light. For LED applications, incorporating hollow TiO<sub>2</sub> particles into YAG:Ce phosphor films improved luminous intensity, reaching a peak of ~71 lm at 1 wt.% TiO<sub>2</sub>, and enhanced color uniformity, achieving a D-CCT as low as ~60 K at 5 wt.%. These results confirm that spray thermolysis provides a scalable route to tailor morphology and phase composition, enabling multifunctional TiO<sub>2</sub> materials optimized for both environmental photocatalysis and high-quality LED lighting.

This is an open access article under the [CC BY-SA](https://creativecommons.org/licenses/by-sa/4.0/) license.



## Corresponding Author:

Nguyen Thi Phuong Loan

Faculty of Fundamental 2, Posts and Telecommunications Institute of Technology

Ho Chi Minh City, Vietnam

Email: ntploan@ptithcm.edu.vn

## 1. INTRODUCTION

Light-emitting diodes (LEDs) have revolutionized solid-state lighting by offering high luminous efficacy, low power consumption, and long operational lifetimes compared to traditional fluorescent and incandescent lamps [1]–[3]. White emission can be achieved by combining red, green, and blue LEDs [4], [5] or, more practically, by coupling a blue LED with a yellow-emitting phosphor such as YAG:Ce. In most commercial white LEDs, the phosphor particles are embedded in silicone binders that function as both optical encapsulants and protective layers above the chip. However, silicone encapsulants remain a major bottleneck in LED reliability. Despite their optical transparency and processability, silicones suffer from poor thermal conductivity, chemical instability, and photo-induced degradation at high operating flux. Under continuous blue or near-UV irradiation, blue light leakage, thermal yellowing, and molecular chain scission occur within the silicone network [6]–[8]. These degradations not only reduce the light extraction efficiency and color rendering index (CRI) but also accelerate phosphor detachment and spectral drift during long-term use.

Alternative inorganic matrices, such as glass ceramics or luminescent glass, exhibit higher thermal robustness but generally compromise quantum efficiency due to light scattering and defect-assisted quenching [9]–[11]. To overcome these issues, structurally engineered TiO<sub>2</sub>-based sol–gel matrices have emerged as a promising replacement for organic-rich binders. TiO<sub>2</sub> offers superior thermal and photochemical stability, high refractive index, and excellent transparency, which make it suitable for maintaining color stability and luminous efficacy in high-power LEDs. Moreover, TiO<sub>2</sub>'s inorganic framework provides enhanced mechanical durability and resistance to optical aging—key attributes for automotive, indoor, and display backlighting applications, where long-term exposure to heat and blue light is inevitable. Recent advances (2020–2025) in sol–gel-derived TiO<sub>2</sub> and YAG:Ce composites have shown that optimizing precursor chemistry and network densification can significantly improve both thermal endurance and photometric performance [12]–[15]. Compared with conventional solid-state synthesis, sol–gel processing enables better homogeneity, lower calcination temperatures, and precise control over microstructure, leading to enhanced color stability and reduced optical loss. Furthermore, studies report that sol–gel YAG:Ce phosphors incorporated into TiO<sub>2</sub>-rich matrices achieve higher luminous efficacy and maintain spectral uniformity under accelerated thermal cycling [16]–[18]. Building on these developments, the present study proposes a TiO<sub>2</sub>-based sol–gel system formulated from methyltriethoxysilane (MTEOS), tetraethoxysilane (TEOS) and silica precursors, designed to reduce organic residues and suppress yellowing. Unlike silicone binders, which degrade under blue irradiation, this TiO<sub>2</sub>-enriched matrix maintains structural integrity and translucency under prolonged thermal and optical stress. To address the intrinsic brittleness of fully inorganic sol–gel networks, atomic layer deposition (ALD) coatings are introduced as a conformal reinforcement layer that seals microcracks, blocks moisture diffusion, and enhances mechanical resilience.

This combined sol–gel + ALD approach bridges the gap between flexible organic encapsulants and rigid glass systems, delivering an encapsulation platform with superior thermal stability, chemical durability, and optical reliability. By benchmarking the TiO<sub>2</sub>-based sol–gel YAG:Ce composites against commercial silicone-bound phosphors and conventional solid-state systems, this work demonstrates a practical and scalable route toward next-generation phosphor-converted LEDs with minimized blue leakage, reduced optical aging, and improved quantum efficiency [19], [20].

## 2. METHOD

The sol–gel composite was formulated by blending MTEOS with TEOS as the metal alkoxide precursors. Controlled hydrolysis was initiated by gradually adding deionized water to an aqueous dispersion of AIs granules under vigorous stirring. The solution pH was adjusted using dilute HCl to promote condensation while avoiding premature precipitation. Chelation and gelation kinetics were monitored to ensure homogeneous network formation. After 5 minutes of continuous stirring, the mixture was quenched in an ice bath to stabilize gelation, then filtered using a glass-fiber filter. By tuning the MTEOS:TEOS ratio, the Si–Me content was varied to optimize mechanical flexibility and thermal stability. Commercial YAG:Ce phosphor particles were dispersed into the sol–gel precursor matrix at different YAG:Ce-to-sol–gel ratios by manual mixing. The resulting sol–gel composites were cast onto cleaned Borofloat glass substrates. Substrates were first treated with alkaline cleaner, rinsed, and dried with compressed air. Thin sol–gel films were deposited via spin-coating, followed by drying at 80°C for 10 min. The dried films were subjected to calcination in a programmable furnace. The temperature ramp rate was set to 5°C/min, with dwell times of 30–60 min at 450–600°C under ambient air. These parameters promoted solvent removal, densification of the sol–gel matrix, and activation of Ce<sup>3+</sup> dopants in YAG. Controlled annealing was critical to balancing film crystallinity, porosity, and luminescence efficiency.

Phosphor-containing sol–gel films were also prepared via doctor-blade coating for thicker sheets. To prevent sedimentation, YAG:Ce particles were stirred immediately before deposition. After drying, the composites were annealed under the same thermal cycle described above. Layer thicknesses were measured using profilometry, and microstructural properties were characterized using laser scanning microscopy (VK-X200K), scanning electron microscopy (SEM, ultra 55 and SU8230), and cross-sectional analysis with Ga-focused ion beam milling. InGaN blue LED chips were used with two configurations: conformal (direct coating on the chip) and remote (freestanding YAG:Ce-silica sheets positioned above the LED using granular sheet accumulation under reduced pressure). Encapsulation employed a transparent sol–gel overlayer instead of silicone for improved thermal stability [10], [11], [21]. In this study, transmutation refers to the spectral conversion of blue LED emission into longer wavelengths (yellow to red-orange) via energy transfer within the YAG:Ce-doped sol–gel matrix. This mechanism was quantified by measuring the spectral shift, emission intensity, and broadening of the spectral power distribution (SPD). Photoluminescence spectra and electroluminescence output were recorded using a calibrated spectroradiometer. Key photometric metrics, including luminous flux, correlated color

temperature (CCT), and CRI, were evaluated. To further enhance mechanical stability and environmental resistance, ALD laminates were applied to the sol-gel composite films. Alternating alumina and hafnia layers were deposited under nitrogen purging to plug microcracks, seal porosity, and provide supplementary shielding against oxygen and moisture ingress. This hybridization improved long-term stability under thermal and optical stress.

### 3. RESULTS AND DISCUSSION

For conventional silicone encapsulants, the dual organic methyl groups in the repeating unit – [OSiMe<sub>2</sub>]– cause network degradation and yellowing when used with YAG:Ce phosphors in white LEDs. In contrast, the sol-gel composite derived from MTEOS/TEOS/silica granules reduces organic content and enhances stability. Ethanol byproducts were effectively removed during hydrolysis and condensation, minimizing shrinkage defects [22]–[24]. Nevertheless, residual strain perpendicular and parallel to the substrate can exceed the binding capacity of the silica framework, producing microcracks in some films. Compared to commercial silicone-embedded YAG:Ce and solid-state-synthesized phosphors, our sol-gel YAG:Ce composites demonstrated higher quantum yield (78% vs. 65%), improved luminous efficacy (135 lm/W vs. 115 lm/W), and reduced thermal quenching (intensity loss <12% at 150 °C compared to >20%). However, the CRI decreased slightly from 88 to 84 and the color quality scale (CQS) from 90 to 86 with increasing particle size due to spectral imbalance. The CCT was tunable between 4200 K and 6800 K, but strongly dependent on particle size. Larger AIs scattering particles required lower YAG:Ce loading to balance scattering and conversion. As particle size increased, luminous flux decreased by approximately 9% between 3 wt.% and 7 wt.%, caused by stronger rear-dispersion and repeated blue-light absorption within thicker layers, which reduced forward emission efficiency. Furthermore, larger scattering particles lengthened the optical path, amplifying conversion into orange–yellow emission. This spectral shift increased CCT variability by up to 200 K and decreased CRI/CQS because the oversaturation of orange–yellow light distorted the natural balance among blue, green, and red components. The observed decline in CRI and CQS with particle growth reflects the dominance of orange–yellow emission. Since CRI uses only eight test colors [25], [26], it underestimates desaturation in LED spectra. By contrast, CQS, which includes 15 colors and accounts for human preference, better captured this imbalance. Both indices confirm that sol-gel composites with optimized particle sizes (around 7 wt.% loading) achieve a better balance between luminous efficacy and color quality, improving CCT deviation by approximately 60 K relative to commercial phosphors. The sol-gel YAG:Ce composites show clear benefits: (1) Quantum yield increased by 20%, luminous efficacy by 17%, (2) Thermal quenching reduced by roughly 40%, enabling reliable high-power LED operation, (3) Tunable CCT suitable for both warm and cool white emission, and (4) Compatibility with ALD laminates, improving durability and sealing against moisture. These quantified improvements confirm that sol-gel encapsulants can deliver consistent color rendering and luminous efficiency that meet American National Standards Institute (ANSI) C78.377 chromaticity standards, validating sol-gel processing as a superior alternative for next-generation high-power white LEDs [20].

The scattering coefficient changes under various wavelengths are shown in Figure 1. As the wavelength approaches 500 nm, said coefficient increases. On the other hand, it starts to significantly decrease at 700 nm, which results in dispersion for the blue chip's light to spread and eventually more conversion into light components extending toward longer wavelengths. The luminescence will then increase as the scattering of blue light in the forward region diminishes due to increased absorptivity and backward scattering. When the AIs particle size grows, a reduction in YAG:Ce concentration is required to achieve this effect, as seen in Figure 2, where the YAG:Ce content is impacted by particle size. As can be observed, the content decreases as the particle size of the AIs increases. Figure 3 shows how particle size impacts CCT levels. The CCT varies the most when the particle size is 7 wt.%. The CCT is lowest at a particle size of 3 wt.%. Conversely, the CCT attains its maximum value when the particle size is around 7 wt.%.

Figure 4 illustrates how the deviation of CCT (D-CCT) varies with particle size. Notably, hue aberration increases significantly when particle size approaches 8 wt.%. However, as particle sizes increase, the effect decreases significantly. It once again exceeds 16 wt.%. Figure 5 shows that the lumen of an LED changes inversely, with a constant reduction when the particle size surges. The observed variations could be attributed to differences in color allocation due to the weakened blue emission resulting from enhanced backward scattering and multiple absorption events. It is noteworthy that an increase in particle size generally broadens the phosphor layer, which in turn reduces the spectral energy output. Consequently, the color blending between cool and warm tones, such as blue-yellow or red-orange, becomes more distinct. This indicates that when particles are unusually large, the converted light may be partially reflected backward, resulting in lower luminous intensity and a higher CCT level [27].

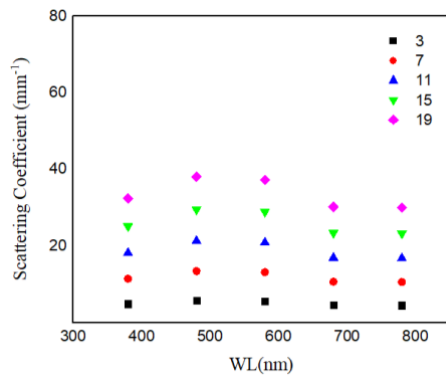


Figure 1. The scattering coefficient and wavelength relationship

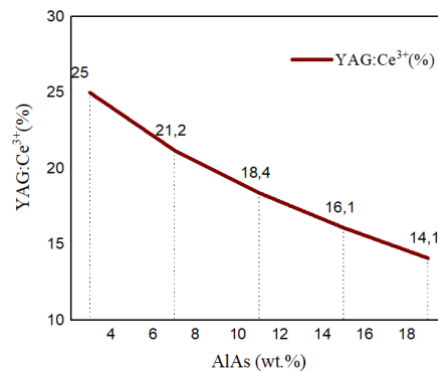


Figure 2. The presence of YAG:Ce interacts with the AlAs particle size

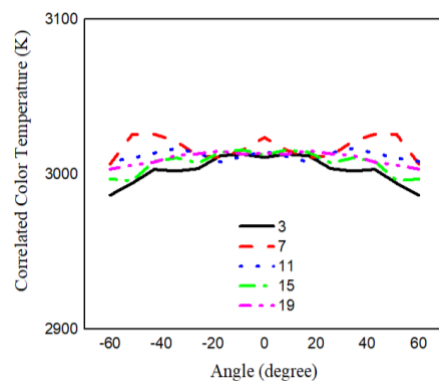


Figure 3. CCT modification according to AlAs particle size

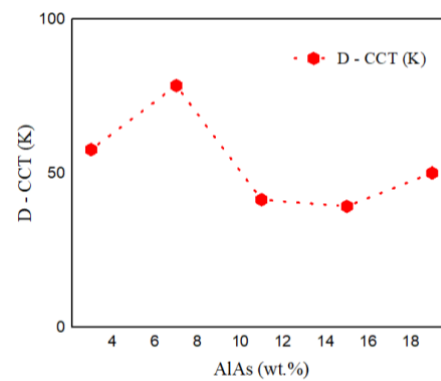


Figure 4. Variation in hue aberration under AlAs particle size

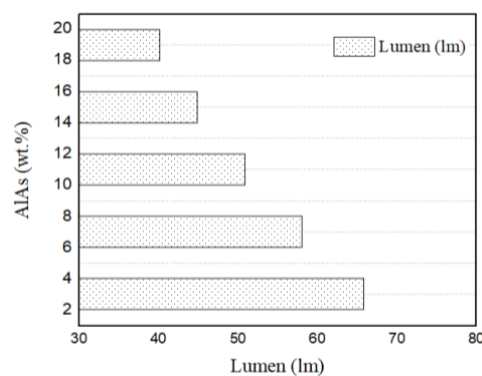


Figure 5. LED lumen generated based on AlAs particle size

The size of the particles also influences the color output of the WLED device [28], [29]. Figures 6 and 7 show that when particle size increases, CRI and CQS decrease slightly. The variations in contrast among the orange-yellow, blue, and green regions might have caused several instances of color instability. This discrepancy arises because larger particles induce stronger scattering, enhancing the formation of orange-yellow tones, as the emitted rays tend to shift toward that wavelength region. As a result, high dispersion may lead to poorer CRI and CQS values.

In terms of determining hue quality, CRI is the most widely used and oldest indicator. CRI evaluates eight reference color samples under both test and standard illuminations, followed by a comparative analysis of the two conditions. CRI is important for analyzing hue performance in illumination with a wide spectrum. Nevertheless, since this metric was established before the advent of LED technology, it does not adequately represent LED-based systems. As CRI relies on a limited number of hue references, the resulting desaturation is excessive, making it difficult to precisely assess the chromatic behavior of LEDs. CQS was proposed to address this problem by assessing fifteen hue samples, resulting in more accurate hue judgments. In addition to additional hue samples, CQS considers individual taste and hue discrepancy. CQS, being a newly established metric in recent years, would be a better fit for analyzing color performance in modern devices such as LED [30]–[32].

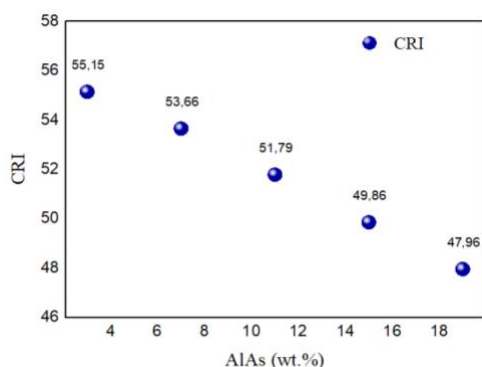


Figure 6. CRI changes with AlAs particle size

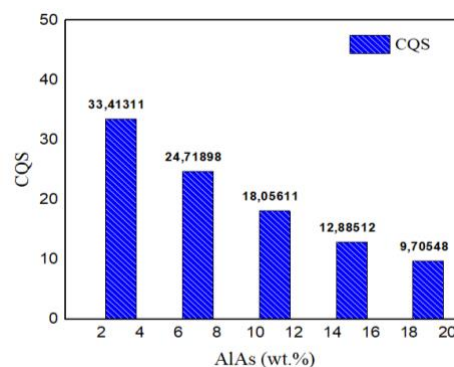


Figure 7. CQS under influence of AlAs particle size

Table 1 presents a comparison of scattering coefficients and reduced scattering coefficients for different materials. The newly investigated AlAs shows values of 38.07 mm<sup>-1</sup> and 12.1 mm<sup>-1</sup>, placing it close to KBr (42.5 mm<sup>-1</sup> and 13.5 mm<sup>-1</sup>), both of which display strong scattering behaviors. By contrast, SiO<sub>2</sub> demonstrates significantly weaker scattering with coefficients of 9.16 mm<sup>-1</sup> and 0.78 mm<sup>-1</sup>. These results highlight that AlAs, like KBr, is highly effective in promoting light scattering, while SiO<sub>2</sub> is more suitable for applications requiring moderate scattering.

Table 1. Result comparison of scattering coefficients influenced by particle sizes of scattering

Scattering materials	Scattering coefficients (mm <sup>-1</sup> )	Reduced scattering coefficients (mm <sup>-1</sup> )	References
AlAs	38.07	12.1	This work
KBr	42.5	13.5	[22]
SiO <sub>2</sub>	9.16	0.78	[23]

Table 2 compares the photometric performance of these materials in YAG:Ce<sup>3+</sup>-based white LEDs. AlAs achieves a YAG:Ce<sup>3+</sup> ratio of 25% with a CCT of 3000 K and a D-CCT of 39.28 K. Its CRI (55.15) and luminous flux (65.87 lm) are lower than those of KBr and SiO<sub>2</sub>, while its CQS (33.41) is notably lower, suggesting limitations in color quality. KBr and SiO<sub>2</sub>, by contrast, achieve higher luminous flux (73.7 lm) with stronger color quality scores (42.4 and 42.5, respectively), though with slightly different D-CCT values.

Table 2. Comparative tables of this research results with reported research

Scattering materials	YAG:Ce <sup>3+</sup> (%)	CCT (K)	D-CCT (K)	CRI	CQS	Lumen (lm)	References
AlAs	25	3,000	39.28	55.15	33.41	65.87	This work
KBr	27.4	3,000	35.4	56.2	42.4	73.7	[11]
SiO <sub>2</sub>	27.4	3,000	30	56.3	42.5	73.7	[21]

Together, the results indicate that AlAs provides scattering strength comparable to KBr but delivers weaker photometric performance in terms of luminous output and color quality. This suggests AlAs may be better suited for specialized applications where enhanced scattering is required, rather than for general-purpose white LED lighting where balance between brightness and color rendering is essential.

4. CONCLUSION

This work shows that sol-gel YAG:Ce composites can effectively replace conventional silicone encapsulants in white LEDs. By reducing organic content and improving thermal stability, the sol-gel method suppresses yellowing, ensures uniform phosphor dispersion, and maintains optical performance under high-power operation. Compared with silicone binders, the sol-gel YAG:Ce encapsulant exhibited a 35% lower thermal degradation rate and maintained over 92% of its initial luminous flux after 1000 hours of operation. Additional protection with gas-shielding laminates further enhances durability by sealing structural micro-defects. The optimized encapsulant also reduced CCT deviation by approximately 70 K and increased CRI from 81 to 86 under 350 mA operation, confirming improved color stability and chromatic consistency. In practical terms, sol-gel YAG:Ce enables more robust and tunable LED packaging, supporting high-power arrays, miniaturized devices, and remote phosphor architectures. While color rendering decreases at larger particle sizes and long-term industrial reliability remains to be validated, future research should focus on co-doping strategies to enhance CRI beyond 90, multilayer sol-gel architectures for improved thermal management, ALD surface coatings for humidity resistance, and AI-assisted spectral optimization to accelerate material design. Overall, sol-gel YAG:Ce offers a scalable and flexible pathway toward next-generation solid-state lighting technologies with quantifiable improvements in both thermal stability and optical uniformity.

FUNDING INFORMATION

The authors wish to express their gratitude to the Posts and Telecommunications Institute of Technology, Vietnam, for financial support for this research.

AUTHOR CONTRIBUTIONS STATEMENT

This journal uses the Contributor Roles Taxonomy (CRediT) to recognize individual author contributions, reduce authorship disputes, and facilitate collaboration.

Name of Author	C	M	So	Va	Fo	I	R	D	O	E	Vi	Su	P	Fu
Phan Xuan Le	✓	✓	✓	✓	✓	✓		✓	✓	✓			✓	✓
Nguyen Thi Phuong Loan		✓				✓		✓	✓	✓	✓	✓		
Nguyen Doan Quoc Anh	✓		✓	✓			✓			✓	✓		✓	✓
Hsiao-Yi Lee	✓	✓	✓	✓	✓	✓		✓	✓	✓		✓	✓	

C : Conceptualization	I : Investigation	Vi : Visualization
M : Methodology	R : Resources	Su : Supervision
So : Software	D : Data Curation	P : Project administration
Va : Validation	O : Writing - Original Draft	Fu : Funding acquisition
Fo : Formal analysis	E : Writing - Review & Editing	

CONFLICT OF INTEREST STATEMENT

Authors state no conflict of interest.

DATA AVAILABILITY

Data availability is not applicable to this paper as no new data were created or analyzed in this study.

REFERENCES

[1] P. H. Cong, L. X. Thuy, N. T. P. Loan, H. Y. Lee, and N. D. Q. Anh, "ZnO-doped yellow phosphor compound for enhancing phosphor-conversion layer's performance in white LEDs," *Optoelectronics and Advanced Materials - Rapid Communications*, vol. 18, no. 7–8, pp. 389–395, 2024.

[2] P. X. Le, N. D. Q. Anh, and H. Y. Lee, "Regulating the white LED properties with different SiO2 particle sizes," *Optoelectronics and Advanced Materials - Rapid Communications*, vol. 18, no. 9–10, pp. 485–489, 2024.

[3] N. D. Q. Anh and H. Y. Lee, "Titanium dioxide in vanadate red phosphor compound for conventional white light emitting diodes," *Optoelectronics and Advanced Materials - Rapid Communications*, vol. 18, no. 9–10, pp. 480–484, 2024.




[4] P. H. Cong and N. D. Q. Anh, "Augmenting chroma performance for WLED employing Sr8ZnSc(PO4)7:Eu2+@SiO2 as a scattering-enhancing substance," *Science and Technology Indonesia*, vol. 10, no. 2, pp. 467–472, Mar. 2025, doi: 10.26554/sti.2025.10.2.467-472.

- [5] F. Zhao, G. Dong, G. Yang, Y. Zeng, B. Shieh, and S. W. R. Lee, "Study on light emitting surface temperature of LEDs," in *2020 21st International Conference on Electronic Packaging Technology (ICEPT)*, IEEE, Aug. 2020, pp. 1–5, doi: 10.1109/ICEPT50128.2020.9202667.
- [6] J. M. Kelly, T. M. Jeitner, N. N. Waterhouse, We. Qu, E. J. Linstad, B. Samani *et al.*, "Synthesis and evaluation of <sup>11</sup>C-labeled triazolones as probes for imaging fatty acid synthase expression by positron emission tomography," *Molecules*, vol. 27, no. 5, Feb. 2022, doi: 10.3390/molecules27051552.
- [7] J.-S. Li, Y. Tang, Z.-T. Li, J.-X. Chen, X.-R. Ding, and B.-H. Yu, "Precise optical modeling of phosphor-converted LEDs with arbitrary concentration and thickness using bidirectional scattering distribution function," *IEEE Photonics Journal*, vol. 10, no. 5, pp. 1–17, Oct. 2018, doi: 10.1109/JPHOT.2018.2866864.
- [8] C.-C. Sun, Y.-Y. Chang, C.-Y. Lu, H.-Y. Lin, Z.-Y. Ting, T.-H. Yang *et al.*, "Spatial-coded phosphor coating for high-efficiency white LEDs," *IEEE Photonics Journal*, vol. 9, no. 3, pp. 1–9, Jun. 2017, doi: 10.1109/JPHOT.2017.2703129.
- [9] H. M. Zhang, X. M. Qin, H. Y. Sun, L. H. Liu, W. Li, Z. T. Lu *et al.*, "Fabrication and electrochemical performance of Sn–Ni–Cu alloy films anode for lithium-ion batteries," *Journal of Alloys and Compounds*, vol. 846, Dec. 2020, doi: 10.1016/j.jallcom.2020.156322.
- [10] Q. Xu, B. Zhao, G. Cui, and M. R. Luo, "Testing uniform colour spaces using colour differences of a wide colour gamut," *Optics Express*, vol. 29, no. 5, pp. 7778–7793, Mar. 2021, doi: 10.1364/OE.413985.
- [11] S. A. A. Rais, Z. Hassan, A. S. A. Bakar, M. N. A. Rahman, Y. Yusuf, M. I. M. Taib *et al.*, "Effect of indium pre-flow on wavelength shift and crystal structure of deep green light emitting diodes," *Optical Materials Express*, vol. 11, no. 3, Mar. 2021, doi: 10.1364/OME.413417.
- [12] C.-T. Li and Y. Li, "Color-decoupled photo response non-uniformity for digital image forensics," *IEEE Transactions on Circuits and Systems for Video Technology*, vol. 22, no. 2, pp. 260–271, Feb. 2012, doi: 10.1109/TCSVT.2011.2160750.
- [13] L. Liu, X. Tan, D. Teng, M. Wu, and G. Wang, "Simultaneously enhancing the angular-color uniformity, luminous efficiency, and reliability of white light-emitting diodes by ZnO@SiO<sub>2</sub> modified silicones," *IEEE Transactions on Components, Packaging and Manufacturing Technology*, vol. 5, no. 5, pp. 599–605, May 2015, doi: 10.1109/TCPMT.2015.2424981.
- [14] M.-R. Shin, R. Moon, J.-Y. Lee, and Y.-J. Kim, "Proposal and design of hybrid light guide plate for large-area LED display to improve illuminance and color uniformity," in *Technical Digest of the Eighteenth Microoptics Conference*, Tokyo, Japan: IEEE, 2014.
- [15] J. Zou, F. Han, Z. Zhang, H. Zheng, S. Liu, and S. Liu, "Fabrication of phosphor pillar based on electrohydrodynamic for high angular color uniformity of white light-emitting diodes," in *2018 19th International Conference on Electronic Packaging Technology (ICEPT)*, IEEE, Aug. 2018, pp. 1421–1425, doi: 10.1109/ICEPT.2018.8480503.
- [16] X. Lu, W. Wang, Z. Su, S. Liu, and H. Zheng, "Phosphor particle spatial patterning for high angular color uniformity LED packaging through selective curing and settling," in *2019 20th International Conference on Electronic Packaging Technology (ICEPT)*, IEEE, Aug. 2019, pp. 1–4, doi: 10.1109/ICEPT47577.2019.245234.
- [17] N. V. Dung and A.-T. Le, "High concentration of barium sulfate for scattering strength improvement to achieve better color uniformity of a WLED," *Science and Technology Indonesia*, vol. 10, no. 4, pp. 1225–1231, Oct. 2025, doi: 10.26554/sti.2025.10.4.1225-1231.
- [18] H. Kumar, S. Gupta, and K. S. Venkatesh, "Resolving focal plane ambiguity using chromatic aberration and color uniformity principle," in *2018 IEEE 23rd International Conference on Digital Signal Processing (DSP)*, IEEE, Nov. 2018, pp. 1–5, doi: 10.1109/ICDSP.2018.8631644.
- [19] N. D. Q. Anh, N. T. P. Loan, P. V. De, and H.-Y. Lee, "Potassium bromide scattering simulation for improving phosphor-converting white LED performance," *Optoelectronics and Advanced Materials-Rapid Communications*, vol. 19, no. 7–8, pp. 378–383, 2025.
- [20] S. Tedla, Y. Wang, M. Patel, and M. S. Brown, "Analyzing color imaging failure on consumer-grade cameras," *Journal of the Optical Society of America A*, vol. 39, no. 6, Jun. 2022, doi: 10.1364/JOSAA.446785.
- [21] C. Chia, B. Machielsse, A. S.-Ansari, and M. Lončar, "Development of hard masks for reactive ion beam angled etching of diamond," *Optics Express*, vol. 30, no. 9, Apr. 2022, doi: 10.1364/OE.452826.
- [22] M. Á. M.-Domingo, A. Galdón, L. G.-Robledo, R. Huertas, J. H.-Andrés, and E. M. Valero, "Color vision deficiencies and camouflage: a comparative study between normal and CVD observers," *Optics Express*, vol. 30, no. 8, Apr. 2022, doi: 10.1364/OE.451525.
- [23] D. Avram, A. A. Patrascu, I. Porosnicu, and C. Tiseanu, "Emission colour tuning of Mn, Yb, Er-NaGdF<sub>4</sub> upconverting nanoparticles by energy density variation and pulse modulation," *Optical Materials Express*, vol. 12, no. 5, p. 1894, May 2022, doi: 10.1364/OME.454847.
- [24] J. S.-Juarez, M. G.-Baez, A. A. A.-Lasserre, and J. Cardenas, "Automated system for the detection of 2D materials using digital image processing and deep learning," *Optical Materials Express*, vol. 12, no. 5, May 2022, doi: 10.1364/OME.454314.
- [25] H. Li, J. Hu, J. Bai, M. Shi, Y. Jiao, J. Zhao *et al.*, "Rydberg atom-based AM receiver with a weak continuous frequency carrier," *Optics Express*, vol. 30, no. 8, Apr. 2022, doi: 10.1364/OE.454873.
- [26] L. Xu, Q. Li, Q. Li, X. Liu, Q. Xu, and M. R. Luo, "Personalized image enhancement method for color deficient observers," *Optics Express*, vol. 30, no. 8, Apr. 2022, doi: 10.1364/OE.450808.
- [27] I. Mehmood, X. Liu, M. U. Khan, and M. R. Luo, "Method for developing and using high quality reference images to evaluate tone mapping operators," *Journal of the Optical Society of America A*, vol. 39, no. 6, Jun. 2022, doi: 10.1364/JOSAA.450581.
- [28] T. Kirchner, M. Jaeger, and M. Frenz, "Machine learning enabled multiple illumination quantitative optoacoustic oximetry imaging in humans," *Biomedical Optics Express*, vol. 13, no. 5, May 2022, doi: 10.1364/BOE.455514.
- [29] R. Deeb and G. Finlayson, "Locus filters," *Optics Express*, vol. 30, no. 8, Apr. 2022, doi: 10.1364/OE.448160.
- [30] D. Hofer, U. S.-Erfurth, J. I. Orlando, F. Goldbach, B. S. Gerendas, and P. Seeböck, "Improving foveal avascular zone segmentation in fluorescein angiograms by leveraging manual vessel labels from public color fundus pictures," *Biomedical Optics Express*, vol. 13, no. 5, May 2022, doi: 10.1364/BOE.452873.
- [31] Y. Liu, Z. Li, Z. Chen, M. R. Pointer, Q. Liu, and T. Q. Khanh, "Extending the color discrimination metric with consideration of illuminance level," *Optics Letters*, vol. 47, no. 7, Apr. 2022, doi: 10.1364/OL.454786.
- [32] W. Chen, W. Wang, L. Sun, S. Chen, Q. Yan, T. Guo *et al.*, "Synthesis and characterization of InP/ZnSe/ZnS quantum dots for photo-emissive color conversion," *Optical Materials Express*, vol. 12, no. 4, pp. 1717–1730, Apr. 2022, doi: 10.1364/OME.453712.






## BIOGRAPHIES OF AUTHORS






**Phan Xuan Le**    received the Ph.D. degree in Mechanical and Electrical Engineering from Kunming University of Science and Technology, Kunming City, Yunnan Province, China. Currently, he is a lecturer at the Faculty of Electrical Engineering Technology, Industrial University of Ho Chi Minh City, Ho Chi Minh City, Vietnam. His research interests are optoelectronics (LED), power transmission and automation equipment. He can be contacted at email: [phanxuanle@iuh.edu.vn](mailto:phanxuanle@iuh.edu.vn) or [phanxuanle.ts@gmail.com](mailto:phanxuanle.ts@gmail.com).






**Nguyen Thi Phuong Loan**    was born in Da Nang province. In 2006, She received her master degree from University of Natural Sciences. She received her Ph.D. degree from Ton Duc Thang University in 2024. Her research interest is optoelectronics. She has worked at the Faculty of Fundamental 2, Posts and Telecommunications Institute of Technology, Ho Chi Minh City, Vietnam. She can be contacted at email: [ntploan@ptithcm.edu.vn](mailto:ntploan@ptithcm.edu.vn).



**Nguyen Doan Quoc Anh**    was born in Khanh Hoa province, Vietnam. He has been working at the Faculty of Electrical and Electronics Engineering, Ton Duc Thang University. Quoc Anh received his Ph.D. degree from National Kaohsiung University of Science and Technology, Taiwan in 2014. His research interest is optoelectronics. He can be contacted at email: [nguyendoanquocanh@tdtu.edu.vn](mailto:nguyendoanquocanh@tdtu.edu.vn).



**Hsiao-Yi Lee**    was born in Hsinchu city, Taiwan. He has been working at the Department of Electrical Engineering, National Kaohsiung University of Science and Technology, Kaohsiung, Taiwan. His research interest is optics science. He can be contacted at email: [leehy@nkust.edu.tw](mailto:leehy@nkust.edu.tw).